The thermoacoustic effect and its application in air-coupled testing of composite structures

Klaas BENTE [1], Daniel KOTSCHATE [1], Saskia WENDLAND [1,2], Mate GAAL [1]
[1] Bundesanstalt für Materialforschung und -prüfung (BAM), Berlin, Germany
[2] Technical University of Ilmenau, Germany

Contact e-mail: klaas.bente@bam.de

Abstract. Airborne ultrasonic testing of lightweight, structured composite materials enables fast and contact-free non-destructive testing in aerospace and avoids material degradation due to contact with a coupling liquid. Established resonant air-coupled transducers consist of piezocomposite materials and several matching layers or more advanced materials like charged cellular polypropylene. The relaxation time and the specific frequency of such mechanical ultrasound emitters limit the spectrum of applications for each device. A short pulse length is key for reliable defect detection and each component at test can be best characterized at material- and geometry-specific frequencies. Here we show that focused thermoacoustic transducers are suited for testing lightweight, structured composite plates. Since the ultrasound is generated in air, these transducers show no resonance behavior and emit a broadband acoustic spectrum between 1.2 kHz and 1 MHz. Composite specimens of 3 mm to 9 mm thickness made of polylactide with a honeycomb structure were tested. Flat bottom holes were introduced to quantify the spatial resolution of the imaging method inside the strongly anisotropic specimen. As no broadband receivers are available yet, cellular polypropylene transducers were used as receivers, which limits the bandwidth of the method towards the bandwidth of the receiver. Nevertheless, we demonstrate the competitiveness of the thermoacoustic transducer compared to mechanical emitters at their respective resonance frequencies. Because a thermoacoustic transmitter features a nearly ideal pulse width, a single transmitter can be coupled with receivers with different resonance frequencies. With the development of broadband ultrasound receivers, air-coupled ultrasound spectroscopy will likely be possible in the near future. The analysed transducer holds the potential to speed up testing during production and maintenance in aerospace and automotives. Its combination with a broadband receiver could also expand the application field of air-coupled ultrasonic testing from a qualitative error detection towards a quantitative, spatially resolved analysis of mechanical material properties.

1. Introduction

Air-coupled ultrasonic material testing has distinct advantages when compared to other non-destructive imaging techniques. These include contactless coupling, no ionizing radiation, manageability and costs [1].

The main limitation of the technique is a high difference in acoustic impedance between air and the imaged object's material [2]. This leads to a high reflectivity and all further signals

inside the object are of relatively low amplitude. Besides this fundamental physical limitation, we would like to point out three more restrictions that prevent this technique from becoming a standard in non-destructive testing in aerospace.

Most air-coupled transducers currently used in industry and developed in science work at a specific resonance frequency due to the thickness mode of vibration of the transducer material. One of the resonant transducer's main disadvantage is the time needed to find a suitable frequency and hence a suitable combination of sending and receiving devices for each set of material parameters and object geometries. The disadvantage of needing many transducer combinations to account for each new material-geometry combination can outweigh the advantages of the technique. Secondly, resonant transducers only enable a qualitative detection of interfaces and no quantification of material properties. Finally, the spatial resolution along the acoustic axis for pulse-echo sequences is low for resonant air-coupled transducers due to the limitation in frequencies that can practically be used in air at practical distances. Sound wave with frequencies above 2 MHz experience heavy damping in air and the resulting width of an acoustic pulse can often be too large to investigate relevant errors.

Broadband, air-coupled ultrasound emitters hold potential to overcome the listed limitations. Broadband pulses feature short pulse widths, which enable more precise echo-based imaging. Additionally, broadband signals might enable airborne ultrasound spectroscopy, facilitating spatially resolved material characterization when combined with broadband receivers [2]–[4]. Further, an ideal transducer would be usable at different frequencies that can be adjusted to the case needed for a certain material and object geometry.

Here, we show for transmission imaging that our broadband emitter [5], [6] can compete with a narrowband transducer that has been chosen for a certain material and object geometry. In the context of aerospace applications, we chose a hardware specimen made of a composite material with an internal honeycomb structure and flat bottom holes. We would like to emphasize that several highly sensitive narrowband transducer combinations were tested and the best performing combination was used for all further experiments. Hence, the broadband transducer competed with the best available solution that our narrowband transducer collection could offer. Thereby, we used a receiver, matched to the narrowband emitter.

We first outline the generation of broadband ultrasound signals with the thermoacoustic (TA) effect, describe how our TA emitter was built, describe the transmission imaging setup and the competing narrowband transducers and finally show and discuss the results.

2. Transducers

2.1 Broadband Acoustic Pulses Using the Thermoacoustic Effect

When heating up a closed volume V of air, the local increase of internal energy ΔU leads to an increase in pressure $p = \Delta U/V$. The resulting peak in pressure travels through air as a longitudinal sound wave [5]. The advantages of this kind of sound generation are self-evident, as no resonant mass has to perform the mechanical volume-work and no resonance frequency is related to the sound generation process. Hence, only the time dependency of

the heat transfer on the surface of the heat generator determines the shape of the sound wave in air.

In order to predict an acoustic pressure, ΔU and V have to be determined. For each surface element of a transducer, one can assume V to be a half-sphere with a radius depending on the heating time and the speed of sound in air. ΔU is the internal energy that is generated inside the transducer and transfered to air. A reliably controllable heat source is a thin ohmic conductor mounted onto a substrate material, such that the available effective power is the electrical power loss inside the resistor. The ratio between the heat transfer towards the substrate, holding the thin ohmic film and air can be determined by considering the thermal properties of the substrate and air, as summarized in the next paragraph.

2.2 Realization of a Focused Thermoacoustic Emitter

A fused silica glass substrate was coated with indium tin oxide (ITO) using physical vapor deposition [5]. The substrate was chosen to maximize chemical, thermal and mechanical stability to achieve a long operating time, while at the same time providing a low thermal effusivity $e = \sqrt{k\rho c}$, where k is the thermal conductivity, ρ is the density and c_p is the specific heat capacity of the substrate material. The effusivity is the material parameter that primarily determines what proportion of the generated heat in the thin film on the material's surface is transferred into the substrate and how much heat reaches the air and causes sound wave generation.

The implemented transducer is displayed in Figure 1. ITO was chosen as a film material due to its relatively large resistance and its chemical and thermal stability, small density and heat capacity. The film thickness was 30 nm to minimize the influence of the time-dependent heat and current distribution inside the conductor.

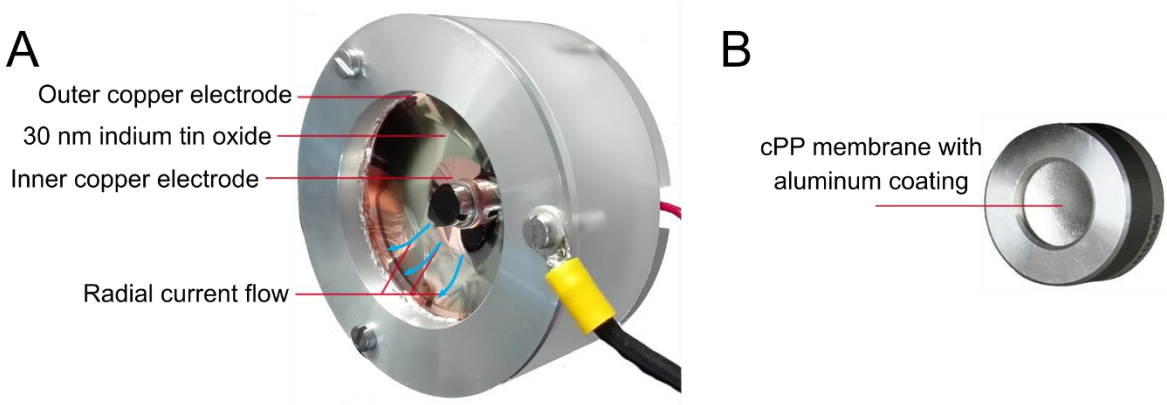

Fig. 1. Labelled photographs of the utilized transducers. **A** Broadband TA transducer. The ITO layer heats the air and the fused silica glass it is deposited on. The locally stored heat in air locally expands the air volume and a wave acoustic pressure wave propagation is initiated at each point on the ITO curved surface. This permits the generation of a focused acoustic field. **B** Cellular polypropylene transducer. The membrane is mounted onto a spherically curved, electrically conductive surface and coated with a 100 nm aluminium film and vibrates at a resonance frequency of 283 kHz.

Copper contacts were locally deposited onto the ITO surface, again using physical vapor deposition. A high voltage pulse generator was connected to the copper contacts. A concentric copper contact arrangement that led to a radial current flow was chosen. The glass substrate featured a spherically curved surface such that a focused acoustic field was generated. The diameter of the outer ITO boundary was 44 mm and the curvature was -92.5 mm.

2.3 Narrowband Reference Emitters

A focused cellular polypropylene (cPP) transducer was used as a reference emitter. These ferroelectret foil transducers feature a resonance frequency that can be adjusted during construction based on their foil thickness and diameter [7], [8]. A focusing shape was achieved by mounting the foil onto an electrically conductive, curved surface [9]. The outer surface was coated with a 100 nm aluminium film. Both surfaces were connected to an electric pulser. A relatively small aperture of 11 mm together with a high resonance frequency of 282 kHz provided the best lateral resolution, such that all relevant features of the hardware specimen were detectable. Due to its resonance behavior the emitter had to be combined with a receiver featuring the same resonance frequency.

2.4 Narrowband Receiver

The reference cPP emitter dictated the choice of the receiving transducer. A twin of the emitting transducer was used with a measured resonance frequency at 283 kHz. The same receiver was used with the TA transducer to directly compare the performance of the broadband emitter.

3. Transmission Imaging Setup

3.1 Hardware Specimen

A 3D-printed, polylactide (PLA) step wedge with flat bottom holes and an internal honeycomb structure and a fill factor of 15 % was imaged (see Figure 2). Further details on such specimen can be found in [10] The specimen was 125 mm wide and high, while the step thicknesses S were 3 mm, 6 mm and 9 mm. Each step included four flat bottom holes with a depth of 1.5 mm, 4.5 mm and 6 mm, respectively, and a width of 2 mm, 4 mm, 6 mm and 10 mm for each depth. The honeycomb parameters are depicted in in Figure 2 and were set to $R = 3$ mm, $t = 1$ mm and $h = S - 2t$. No honeycomb infill was produced below the flat bottom holes of the 6 mm and 3 mm thick steps due to the small thickness of the remaining material.

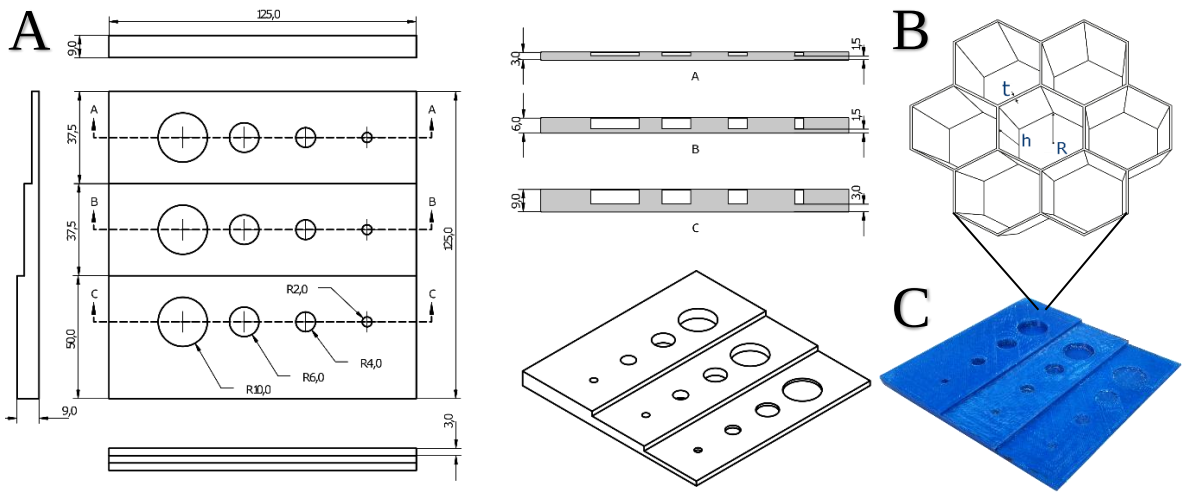

Fig. 2. The hardware specimen was designed to investigate the resolution of both the narrowband-narrowband and the broadband-narrowband transmission imaging technique. **A** Different material thicknesses, flat bottom hole diameters and depths were introduced. **B** A honeycomb infill with a fill-factor of 0.15 was incorporated. **C** The specimen was 3D printed using PLA.

3.2 Imaging Setup and Parameters

Acoustic emitter and receiver were mounted onto an automated positioning system and positioned on both sides of the specimen, facing the specimen. The distance for each transducer was adjusted such that its near field ended at the centre of the middle step's thickness. These were 24 mm for both cPP transducers and 50 mm for the TA transducer. The plate was mounted onto aluminium stacks and the edges were laminated with ultrasound-proof modelling clay to minimize deflection artefacts. The data acquisition and positioning system were part of a commercially available system (USPC 4000 AirTech; Ingenieurbüro Dr. Hillger, Ultrasonic-Techniques). The manipulator was used to scan the area of interest with a 0.3 mm step size while pulsing the emitters with pulse widths of 1.76 µs for the cPP transducer and 2 µs for the broadband transducer. No averaging was necessary while the cPP emitter was used and 3 averages were acquired for each manipulator position for the TA transducer. One and three pulses and 60 dB and 85 dB pre-amplification were used for cPP and TA emitters, respectively.

3.3 Signal and Image Processing

C-scans and D-scans were generated using the Hillgus software (Ingenieurbüro Dr. Hillger, Ultrasonic-Techniques). Thereby, only the first emerging time signal was analysed to avoid influences of reflections and diffractions. While no further processing was necessary for the cPP emitter experiment, an additional IIR bandpass (Butterworth, 4^{th} order, 200 kHz – 350 kHz) filter was needed for the TA experiment. This was necessary to reduce the influence out the remaining acoustic transfer function of the receiving cPP transducer and to damp signals that did not belong to the resonance behavior of around 280 kHz of the receiver.

After image reconstruction, the TA images showed a strong Gaussian noise, which could be removed by a total variation (TV) regularization. It was performed with a μ-parameter of 0.4 and 0.8 for the C-scan and D-scan respectively. A standardised normal noise distribution was assumed and discretised into 9x9 elements and all further TV-parameters were set to standard values according to [11].

4. Comparison of Narrowband and Broadband Imaging Results

The reconstruction results are displayed in Figure 3. C-scans and D-scans were chosen due to best visualization of the honeycomb structure and the flat bottom holes.

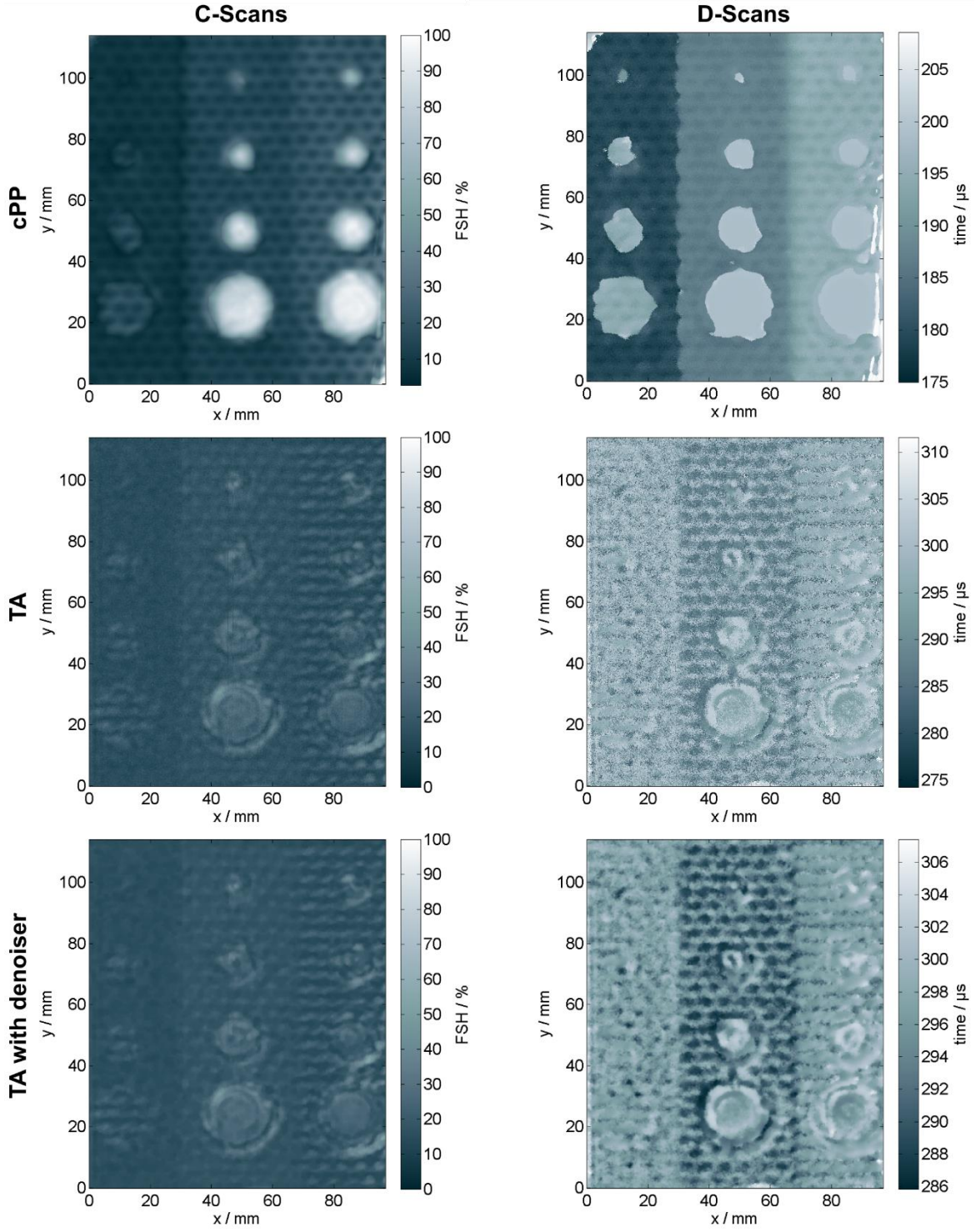

Fig. 3. Ultrasound transmission imaging results of a PLA hardware specimen with different thicknesses, differently sized flat bottom holes and a honeycomb infill. A narrowband cPP emitter and a frequency-matched cPP receiver were used and the performance of a broadband TA emitter with the same receiver compared.

4.1 cPP Performance

The C-scan clearly shows the honeycomb infill and all flat bottom holes with exception of the 1.5 mm deep and 2 mm wide hole. The D-scan shows all holes while still displaying the internal structure.

4.2 TA Performance

The TA scans display strong noise. It was reduced by using the described TV regularization. The denoised C-scan shows the honeycomb structure at 6 mm and 3 mm sample thickness (3 mm is also the thickness of the remaining material below the flat bottom holes at 9 mm step thickness). The amplitudes are inverted when compared to the cPP images. The best honeycomb images were produced at the central 6 mm thick step in the D-scan. Note, that the TA distance to the sample was adjusted at this thickness.

5. Discussion and Outlook

The difference sign in grayscale amplitude in the cPP and TA C-scans could most likely occur due to the difference in excitation pulse forms, since most other parameters are similar between the two setups - including the beam diameter. For both emitters, the receiver was an 11 mm cPP transducer, such that a comparable spatial resolution could be achieved, but the TA transducer is likely to have introduced material-dependent interferences.

The experiment was set up in a way that the cPP transducers would perform well. Thereafter it was tested whether the cPP emitter could be replaced by a TA transducer. The results show that we succeeded up to a material thickness of 6 mm. Thicker material could not be imaged since we filtered the transmitted signal using the transfer function of the receiver and by an IIR bandpass filter. We hence neglected most of the transmission signal's spectrum and energy. It is hence prospective that with more development, a single TA transducer could in future be used to replace several narrowband emitters.

Most promising development include a reduction in size of the TA transducer to increase the spatial resolution of the technique. This will, however, be accompanied by a reduction in material penetration depth due to the reduced output power, which scales linearly with the transducer's surface area.

With the advancement of broadband acoustic receivers it might be possible to locally characterize mechanical material properties using transmission ultrasound spectroscopy.

References

[1] M. C. Remillieux, B. E. Anderson, T. J. Ulrich, P.-Y. Le Bas, M. R. Haberman, and J. Zhu, “Reiview of air-coupled transduction for nondestructive testing and evaluation,” *Acoust. Today*, vol. 10, no. 3, pp. 36–45, 2011.

[2] M. Gaal and D. Kotschate, “New technologies for air-coupled ultrasonic transducers,” in *Proceeding of the 12th European Conference of Non-destructive Testing*, 2018.

[3] J. Grager, D. Kotschate, J. Gamper, M. Gaal, and K. Pinkert, “Advances in air-coupled ultrasonic testing combining an optical microphone with novel transmitter concepts,” in *Proceeding of the 12th European Conference of Non-desstructive Testing*, 2018, pp. 1–10.

[4] M. Daschewski, M. Kreutzbruck, and J. Prager, “Influence of thermodynamic properties of a thermo-acoustic emitter on the efficiency of thermal airborne ultrasound generation,” *Ultrasonics*, vol. 63, pp. 16–22, 2015.

[5] M. Daschewski, R. Boehm, J. Prager, M. Kreutzbruck, and A. Harrer, “Physics of thermo-acoustic sound generation,” *J. Appl. Phys.*, vol. 114, no. 11, 2013.

[6] M. Daschewski, M. Kreutzbruck, J. Prager, E. Dohse, M. Gaal, and A. Harrer, “Resonanzfreie Messung und Anregung von Ultraschall,” *Tech. Mess.*, vol. 82, no. 3, pp. 156–166, 2015.

[7] M. Paajanen, J. Lekkala, and K. Kirjavainen, “ElectroMechanical Film (EMFi) - a new multipurpose electret material,” *Sensors Actuators, A Phys.*, vol. 84, no. 1, pp. 95–102, 2000.

[8] G. M. Sessler and J. Hillenbrand, “Electromechanical response of cellular electret films,” *Appl. Phys. Lett.*, vol. 75, no. 21, pp. 3405–3407, 1999.

[9] M. Gaal, J. Bartusch, E. Dohse, F. Schadow, and E. Köppe, “Focusing of ferroelectret air-coupled ultrasound transducers,” in *AIP Conference Proceedings*, 2016, vol. 1706.

[10] D. Kotschate, S. Wendland, M. Gaal, “Airborne testing of moulded polymer compounds,” in Proceedings of 10th International Symposium on NDT in aerospace, accepted

[11] S.H. Chan, R. Khoshabeh, K.B. Gibson, P.E. Gill, and T.Q. Nguyen, “An augmented Lagrangian method for total variation image restoration,“ *IEEE Trans. Image Process.*, vol. 20, no. 11, pp. 3097–3111, 2011